Geochemical Perspectives Letters

Exchange catalysis during anaerobic methanotrophy revealed by $^{12}CH_2D_2$ and $^{13}CH_3D$ in methane

J.L. Ash[1*], M. Egger[2,#], T. Treude[3,4], I. Kohl[3], B. Cragg[4], R.J. Parkes[4], C.P. Slomp[5], B. Sherwood Lollar[6], E.D. Young[3*]

doi: 10.7185/geochemlet.1910

Abstract

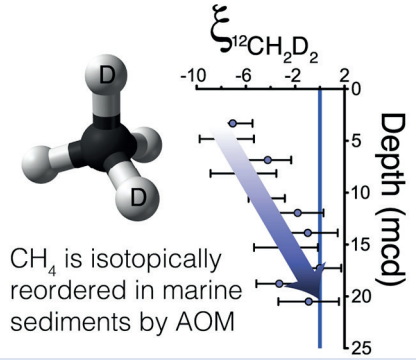

The anaerobic oxidation of methane (AOM) is a crucial component of the methane cycle, but quantifying its role *in situ* under dynamic environmental conditions remains challenging. We use sediment samples collected during IODP Expedition 347 to the Baltic Sea to show that relative abundances of $^{12}CH_2D_2$ and $^{13}CH_3D$ in methane remaining after microbial oxidation are in internal, thermodynamic isotopic equilibrium, and we attribute this phenomenon to the reversibility of the initial step of AOM. These data suggest that $^{12}CH_2D_2$ and $^{13}CH_3D$ together can identify the influence of anaerobic methanotrophy in environments where conventional bulk isotope ratios are ambiguous, and these findings may lead to new insights regarding the global significance of enzymatic back reaction in the methane cycle.

Received 7 May 2018 | Accepted 22 February 2019 | Published 15 April 2019

Letter

Quantifying the subsurface carbon cycle by linking biogeochemistry to deep biosphere metabolisms remains a long-standing challenge compounded by slow rates of reaction (Edwards *et al.*, 2012; Marlow *et al.*, 2017). Even in well-characterised environments, determining how methanogens and anaerobic methanotrophs influence organic matter degradation can be challenging (Regnier *et al.*, 2011; Beulig *et al.*, 2018). These challenges are due in part to how methane produced by methanogens inherits characteristics from its substrates (both a range of organic and inorganic carbon) (Conrad, 2005), and they are further complicated when methane is itself the substrate during anaerobic methane oxidation (AOM) (Whiticar, 1999). Our understanding of how anaerobic methanotrophs respond to varying environmental conditions (Holler *et al.*, 2009, 2011; Yoshinaga *et al.*, 2014) and how they might contribute to "cryptic cycles" (the rapid production and consumption of reactive intermediates) in the marine subsurface is constantly evolving (Egger *et al.*, 2018).

AOM is thought to be carried out by a consortium of methane oxidising archaea and sulphate reducing bacteria performing the net reaction $CH_4+SO_4^{2-} \rightarrow HCO_3^-+HS^-+H_2O$ (Boetius *et al.*, 2000). Evidence suggests that these processes can be decoupled (Milucka *et al.*, 2012; Scheller *et al.*, 2016) and metal oxides may also act as terminal electron acceptors (Beal *et al.*, 2009; Cai *et al.*, 2018). In all cases, the first step of AOM involves C-H bond activation by a modified methyl-coenzyme M reductase (Mcr), the terminal enzyme in methanogenesis (Scheller *et al.*, 2010). Anaerobic methanotrophs use enzymes homologous to those used by methanogens (Krüger *et al.*, 2003; Shima *et al.*, 2012), prompting questions regarding the directionality of these metabolisms (Lloyd *et al.*, 2011; Beulig *et al.*, 2019).

Coupling exploration of methane enzymatic chemistry with isotope geochemistry can provide powerful insights. Here, we interrogate subsurface methane metabolisms by precisely determining concentrations of molecules containing two heavy isotopes, referred to as "clumped" isotopologues (Eiler, 2007). The relative proportions of $^{13}CH_3D$ and $^{12}CH_2D_2$ (reported as $\Delta^{13}CH_3D$ and $\Delta^{12}CH_2D_2$ values relative to a random distribution of isotopes among all CH_4 isotopologues; see Supplementary Information) have known temperature sensitive equilibrium concentrations and thus are sensitive indicators of reversibility in reactions (Piasecki *et al.*, 2016). For instance, axenic cultures of methanogens produce methane

1. Department of Earth, Environmental and Planetary Sciences, Rice University, Houston Texas, USA
2. Center for Geomicrobiology, Aarhus University, Aarhus, Denmark
3. Department of Earth, Planetary, and Space Sciences, UCLA, Los Angeles CA, USA
4. School of Earth and Ocean Sciences, Cardiff University, Cardiff, UK
5. Department of Earth Sciences-Geochemistry, Utrecht University, Utrecht, The Netherlands
6. Department of Earth Sciences, University of Toronto, Toronto Ontario, Canada
now at The Ocean Cleanup Foundation, Rotterdam, The Netherlands
* Corresponding author (email: jeanine.ash@rice.edu; eyoung@epss.ucla.edu)

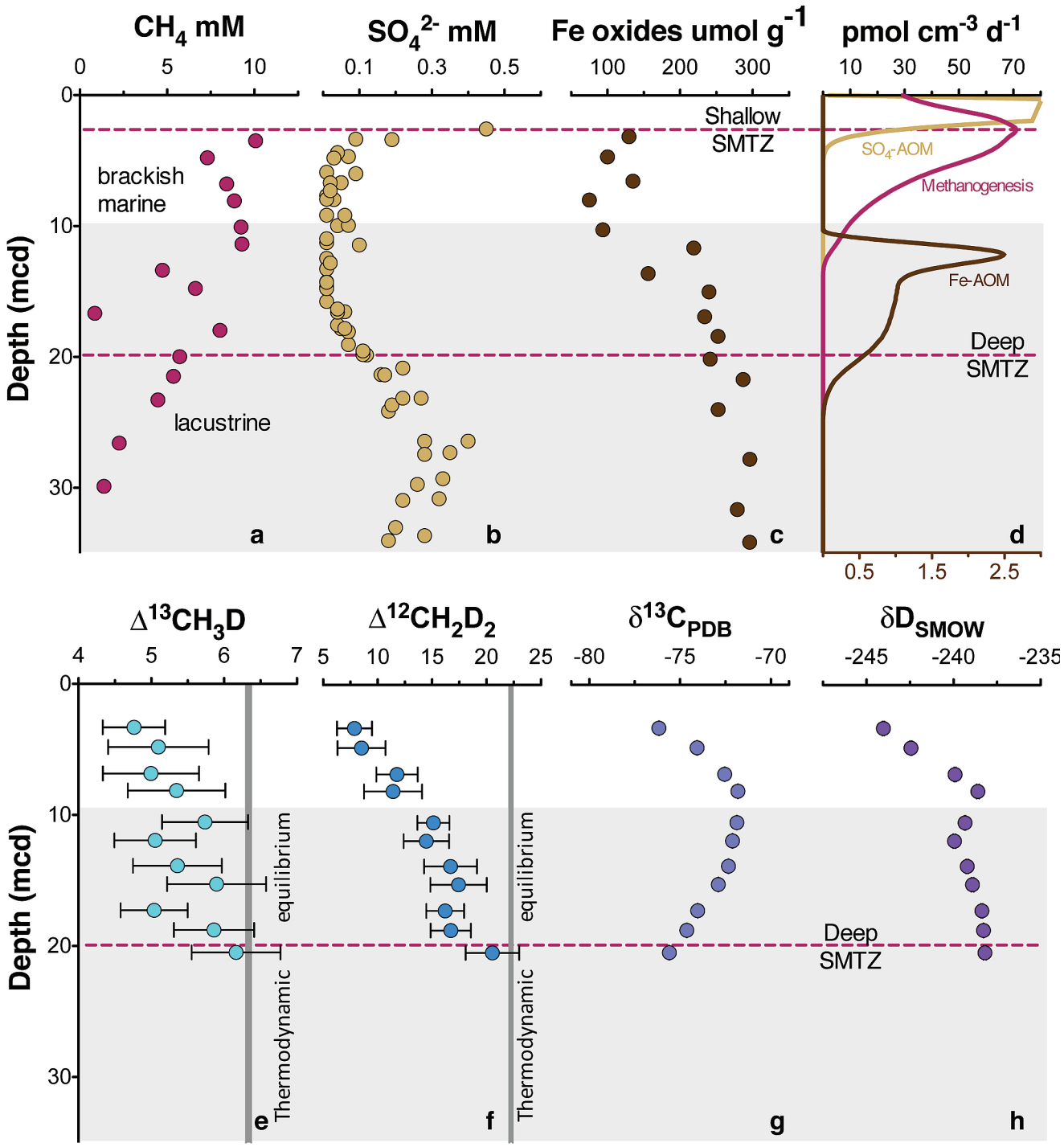

Figure 1 Geochemical profiles (±2 σ) from Bornholm Basin from 3-35 MCD. Horizontal grey bar denotes sediments deposited during lacustrine conditions overlain with sediments deposited during brackish marine conditions. Samples were not recovered above the shallow SMTZ. Pink dashed lines denote a shallow (3.3 MCD) and deep (19.8 MCD) SMTZ; only the shallow SMTZ is shown in the bottom panel for clarity. Dark grey vertical bars in **e** and **f** denote equilibrium isotopologue compositions for the subsurface temperature of 7.8 ± 0.6 °C. Modelled CH_4 production, Fe-AOM and SO_4-AOM rates are shown in panel **d** (Dijkstra *et al.*, 2018). CH_4 production (purple) and SO_4-AOM (gold) rates correspond with the upper x axis and Fe-AOM rates (brown) correspond with the lower x axis. SO_4-AOM rates above the upper SMTZ are calculated using bottom water SO_4 concentrations of 15.0 mM. Additional porewater data shown in Supplementary Information.

with depletions in clumped isotopes relative to the random distribution that reflect kinetic processes (Stolper *et al.*, 2015; Wang *et al.*, 2015; Douglas *et al.*, 2016; Young *et al.*, 2017; Gruen *et al.*, 2018). In some cases, the clumped isotope composition of environmental microbial methane is consistent with the axenic cultures, but in others it displays a clumped isotope composition reflective of equilibration within the environment of formation (Wang *et al.*, 2015; Young *et al.*, 2017). This span in clumped isotope distributions suggests that enzymatic reactions associated with methanogenesis and methanotrophy are capable of ranging from reversible to kinetic. Previous work using one rare isotopologue ($\Delta^{13}CH_3D$) suggests that the rate of methanogenesis controls the degree of molecular isotopic equilibrium (Stolper *et al.*, 2015; Wang *et al.*, 2015). However, the inability to produce equilibrated methane from axenic cultures has led to speculation that AOM may be responsible for equilibrated environmental methane (Stolper *et al.*, 2015; Wang *et al.*, 2016; Young *et al.*, 2017; Gruen *et al.*, 2018). The use

of a second rare isotopologue, $^{12}CH_2D_2$, aids in interpreting the causes of intra-methane disequilibrium and suggests that microbial methanogenesis does not lead to isotopologue equilibrium among methane molecules.

Here, we examine microbial methane from the Bornholm Basin (Baltic Sea; see Supplementary Information) to test the hypothesis that methane remaining after anaerobic oxidation is in thermodynamic equilibrium due to reversibility of the initial step of AOM. We compare methane clumped isotope composition to geochemical profiles (Andrén *et al.*, 2015; Egger *et al.*, 2017) and present day rates of methanogenesis and methanotrophy calculated with a multicomponent diagenetic model (Dijkstra *et al.*, 2018) to determine parameters controlling the isotopic composition of methane (Fig. 1a-d). Methane $\delta^{13}C$ and δD, $\delta^{13}C_{DIC}$, $\delta^{13}C_{TOC}$ and δD_{H2O} vary non-monotonically over 30 metres below seafloor (Fig. 1g,h; Fig. S-1) while $\Delta^{13}CH_3D$ and $\Delta^{12}CH_2D_2$ values increase with depth (Fig. 1e,f).

Comparisons of the bulk isotopic composition of methane to carbon and hydrogen reservoirs at this location are complicated by the change from limnic to marine deposition (Egger *et al.*, 2017). For instance, the hydrogen isotopes in methane are seemingly not equilibrated with porewater that changes by >100 ‰ in this interval (Fig. S-1), obscuring the history of this reservoir. Instead, we will focus on the intra-molecular isotopic equilibrium of the methane itself using clumped isotopes, thus sidestepping the complications in bulk isotope ratios. We introduce $\xi_{^{12}CH_2D_2}$, a parameter that quantifies the degree of thermodynamic disequilibrium for a methane system. $\xi_{^{12}CH_2D_2}$ is analogous to the symbol for the reaction progress variable ($\xi_{^{12}CH_2D_2} = \Delta^{12}CH_2D_{2,\,measured} - \Delta^{12}CH_2D_{2,\,equilibrium}$, see Supplementary Information). Values for $\xi_{^{12}CH_2D_2}$ in upper sediments as low as -7.5 ‰ are significantly different (>6 σ) from 0 ‰ (*i.e.* thermodynamic equilibrium) which is approached with depth (Fig. 2). In order to determine how methanogenesis and methanotrophy influence this transition, we consider evidence for and against reversibility in each metabolism.

Methanogenesis in intra-molecular isotopic thermodynamic equilibrium requires reversibility at the final hydrogen addition step. Trace methane oxidation (TMO) does occur during methanogenesis, but altering the concentration of H_2 or terminal electron acceptors necessary for oxidising methane does not increase TMO and has never been shown to consume greater than ~3 % of the CH_4 produced (Moran *et al.*, 2005; Moran *et al.*, 2007). Although some of the first steps of methanogenesis may be reversible (Valentine *et al.*, 2004), the final transfer of the methyl group to coenzyme M and the subsequent final hydrogen addition are believed to be irreversible (Gärtner *et al.*, 1994; Thauer, 2011). Work on determining the biochemical pathways of Fe(III) reducing ANME has so far required genetically modifying a methanogen, *M. acetivorans* with the Mcr from an ANME-1 group organism because unmodified *M. acetivorans* are unable to be cultured on methane without the modified Mcr (Soo *et al.*, 2016; Yan *et al.*, 2018).

In contrast, AOM is known to have an enzymatic back reaction that suggests the first step of anaerobic methanotrophy is partially reversible, providing a potential mechanism for equilibrating methane isotopologues with environmental temperatures. This back reaction is sensitive to concentrations of the terminal electron acceptor SO_4^{2-} (Holler *et al.*, 2011; Yoshinaga *et al.*, 2014). At high concentrations of SO_4^{2-}, the back reaction produces 3-7 % of the CH_4 consumed by AOM, and at low concentrations of SO_4^{2-} (below 0.5 mM), back reaction can produce as much as 78 % of the CH_4 consumed by AOM (Yoshinaga *et al.*, 2014; Timmers *et al.*, 2017). Intra-cellular exposure of methane to Mcr can lead to isotope exchange catalysis during bond rupture and reformation (Marlow *et al.*, 2017), and methane that diffuses back out of the cell could move an environmental reservoir of methane towards thermodynamic equilibrium. Using estimates of AOM rates from Dijkstra *et al.* (2018), we calculate the timescale of this equilibration (see Supplementary Information) to be on the order of 10^3-10^4 years, consistent with the estimated age of methane at 20 MCD of <~8000 years (Figs. S-1, S-2). Such timescales would vary in environments with differing rates of AOM.

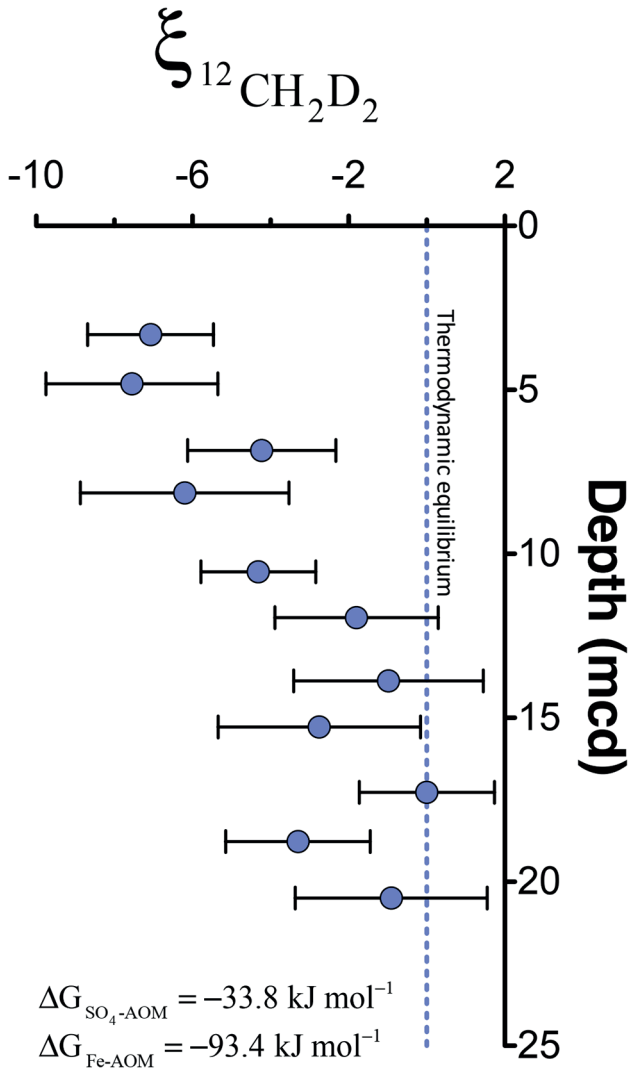

Figure 2 $\xi_{^{12}CH_2D_2}$ values (±2 σ) are the most negative at shallow MCD, indicating the greatest departure from equilibrium and approach zero (violet dashed line) with increasing MCD, indicating an approach towards intra-species thermodynamic equilibrium. ΔG values for SO_4-AOM and Fe-AOM suggest either metabolism is capable of reversibility (see Supplementary Information).

Our findings suggest that when terminal electron acceptors are limiting, equilibrium bond ordering may be used to identify AOM activity even when the bulk isotopic composition of reservoir material is changing and ambiguous. Methane from Kidd Creek Mine (Ontario, Canada) also shows methane isotopologues transitioning with time from non-equilibrated to equilibrated (Fig. 3). This suggests that as energy-rich fractures open, Mcr exposure during the initial step of AOM catalytically exchanges isotopes leaving behind a reservoir that moves closer to thermodynamic equilibrium (Young *et al.*, 2017).

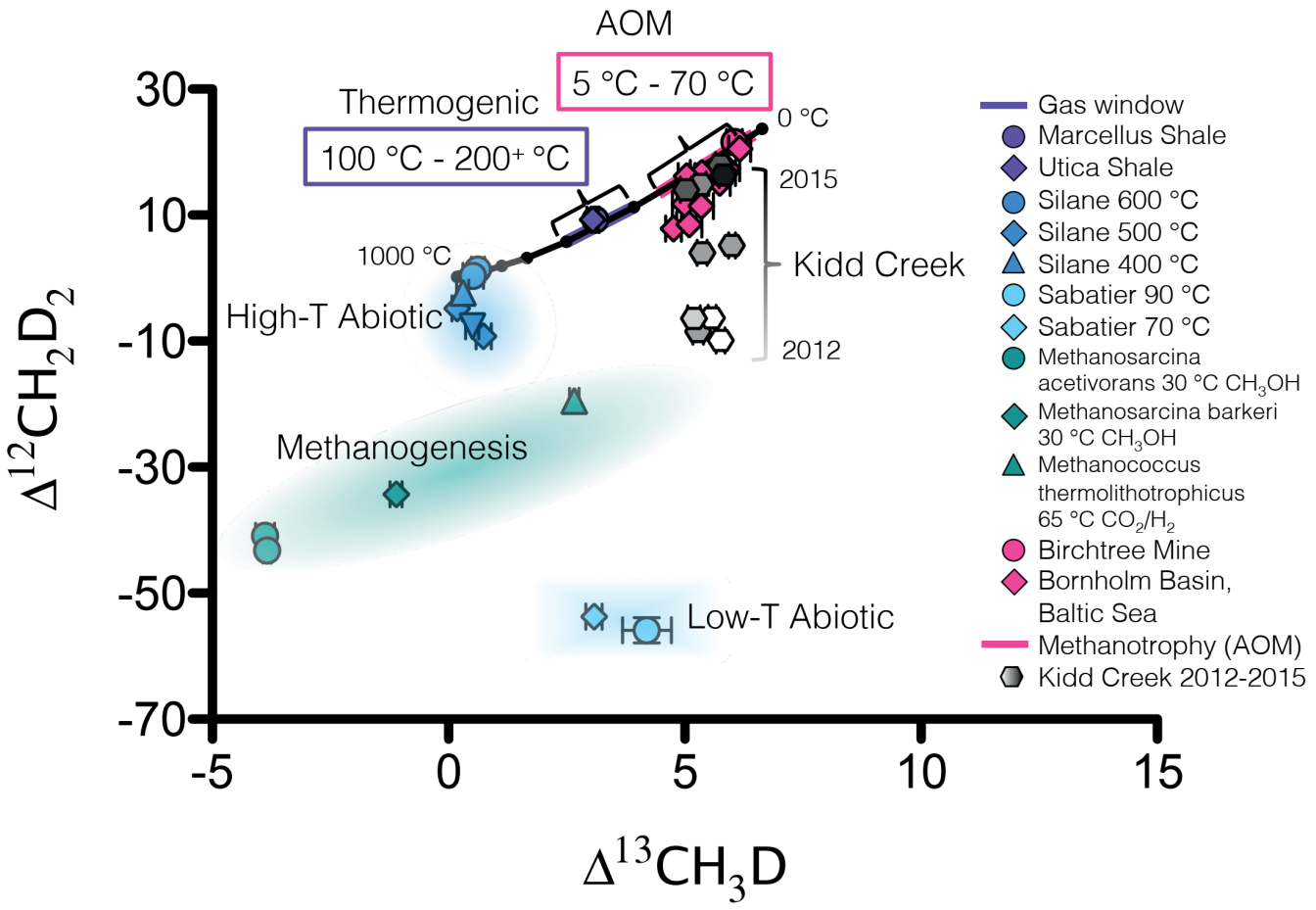

Figure 3 $\Delta^{12}CH_2D_2$ is plotted *versus* $\Delta^{13}CH_3D$. The solid black line represents theoretical thermodynamic equilibrium abundances (with dots representing 100 °C increments from 0-1000 °C). Methane produced by thermogenesis, high temperature abiotic reactions, microbial methanogenesis and low temperature abiotic reactions inhabit unique zones in double isotopologue space. AOM, equilibrating through exchange catalysis during enzymatic back reaction, also inhibits a unique zone: low temperature intra-species thermodynamic equilibrium. Bornholm Basin data (magenta diamonds) span between the methanogenesis and AOM zones, while data from Kidd Creek Mine (black to white symbols) (Young *et al.*, 2017) span from the abiotic to AOM zone. See Supplementary Information for additional sample description.

Methane remaining after AOM is in low temperature equilibrium due to exchange catalysis by Mcr. Therefore, it has distinct $\Delta^{13}CH_3D$ and $\Delta^{12}CH_2D_2$ concentrations when compared to methane produced through other known mechanisms (thermogenesis, microbial methanogenesis and abiotic methanogenesis) (Fig. 3). AOM metabolisms have been shown to be active from -1 °C to 70 °C (Niemann *et al.*, 2006; Holler *et al.*, 2011), a range of temperatures that is unique and distinguishable from equilibrated thermogenic methane forming in the 100 °C to 250 °C gas window. Abiotic methane may also form at low temperatures, yet even when it is apparently equilibrated in $\Delta^{13}CH_3D$, it may exhibit large depletions in $\Delta^{12}CH_2D_2$ that distinguish it from methane that has undergone exchange catalysis during AOM. We suggest that when combined (as in the $\xi_{^{12}CH_2D_2}$ parameter), $\Delta^{12}CH_2D_2$ and $\Delta^{13}CH_3D$ values are sensitive indicators of the degree of thermodynamic equilibrium that may be useful in determining the role of enzymatic back reaction during AOM in the global methane cycle.

Acknowledgements

We thank five anonymous reviewers for helpful critiques as well as Laurence Yeung and Edwin Schauble for conversations and advice on early versions of this manuscript. JLA was funded by an NSF GRFP (DGE – 1144087) while this work was ongoing. We thank the crew and technical staff of the Greatship Manisha. This research used samples and/or data provided by the International Ocean Discovery Program (IODP). Funding for this research was provided to JLA and TT by the Deep Carbon Observatory's Deep Energy Committee.

Editor: Liane G. Benning

Additional Information

Supplementary Information accompanies this letter at http://www.geochemicalperspectivesletters.org/article1910.

Cite this letter as: Ash, J.L., Egger, M., Treude, T., Kohl, I., Cragg, B., Parkes, R.J., Slomp, C.P., Sherwood Lollar, B., Young, E.D. (2019) Exchange catalysis during anaerobic methanotrophy revealed by 12CH2D2 and 13CH3D in methane. *Geochem. Persp. Let.* 10, 26–30.

References

Andrén, T., Jorgensen, B., Cotterill, C., Green, S., Andrén, E., Ash, J., Bauersachs, T., Cragg, B., Fanget, A., Fehr, A. (2015) Expedition 347 Baltic Sea Paleoenvironment. *Proceedings of the Integrated Ocean Drilling Program* 347, 1-66.

Beal, E.J., House, C.H., Orphan, V.J. (2009) Manganese-and iron-dependent marine methane oxidation. *Science* 325, 184-187.

Beulig, F., Røy, H., Glombitza, C., Jørgensen, B. (2018) Control on rate and pathway of anaerobic organic carbon degradation in the seabed. *Proceedings of the National Academy of Sciences* 115, 367-372.

Beulig, F., Røy, H., McGlynn, S., Jørgensen, B. (2019) Cryptic CH4 cycling in the sulfate-methane transition of marine sediments apparently mediated by ANME-1 archaea. *The ISME Journal* 13, 250-262.

Boetius, A., Ravenschlag, K., Schubert, C.J., Rickert, D., Widdel, F., Gieseke, A., Amann, R., Jørgensen, B.B., Witte, U., Pfannkuche, O. (2000) A marine microbial consortium apparently mediating anaerobic oxidation of methane. *Nature* 407, 623-626.

Cai, C., Leu, A.O., Xie, G.-J., Guo, J., Feng, Y., Zhao, J.-X., Tyson, G.W., Yuan, Z., Hu, S. (2018) A methanotrophic archaeon couples anaerobic oxidation of methane to Fe (III) reduction. *The ISME Journal* 12, 1929-1939.

Conrad, R. (2005) Quantification of methanogenic pathways using stable carbon isotopic signatures: a review and a proposal. *Organic Geochemistry* 36, 739-752.

Dijkstra, N., Hagens, M., Egger, M., Slomp, C.P. (2018) Post-depositional vivianite formation alters sediment phosphorus records. *Biogeosciences* 15, 861-883.

Douglas, P., Stolper, D., Smith, D., Anthony, K.W., Paull, C., Dallimore, S., Wik, M., Crill, P.M., Winterdahl, M., Eiler, J. (2016) Diverse origins of Arctic and Subarctic methane point source emissions identified with multiply-substituted isotopologues. *Geochimica et Cosmochimica Acta* 188, 163-188.

Edwards, K.J., Becker, K., Colwell, F. (2012) The deep, dark energy biosphere: intraterrestrial life on earth. *Annual Review of Earth and Planetary Sciences* 40, 551-568.

Egger, M., Hagens, M., Sapart, C.J., Dijkstra, N., van Helmond, N.A., Mogollón, J.M., Risgaard-Petersen, N., van der Veen, C., Kasten, S., Riedinger, N. (2017) Iron oxide reduction in methane-rich deep Baltic Sea sediments. *Geochimica et Cosmochimica Acta* 207, 256-276.

Egger, M., Riedinger, N., Mogollón, J.M., Jørgensen, B.B. (2018) Global diffusive fluxes of methane in marine sediments. *Nature Geoscience* 11, 421.

Eiler, J.M. (2007) "Clumped-isotope" geochemistry -- The study of naturally-occurring, multiply-substituted isotopologues. *Earth and Planetary Science Letters* 262, 309-327.

Gärtner, P., Weiss, D.S., Harms, U., Thauer, R.K. (1994) N5-Methyltetrahydromethanopterin: Coenzyme M Methyltransferase from Methanobacterium thermoautotrophicum. *The FEBS Journal* 226, 465-472.

Gruen, D.S., Wang, D.T., Könneke, M., Topçuoğlu, B.D., Stewart, L.C., Goldhammer, T., Holden, J.F., Hinrichs, K.-U., Ono, S. (2018) Experimental investigation on the controls of clumped isotopologue and hydrogen isotope ratios in microbial methane. *Geochimica et Cosmochimica Acta* 237, 339-356.

Holler, T., Wegener, G., Knittel, K., Boetius, A., Brunner, B., Kuypers, M.M., Widdel, F. (2009) Substantial 13C/12C and D/H fractionation during anaerobic oxidation of methane by marine consortia enriched in vitro. *Environmental Microbiology Reports* 1, 370-376.

Holler, T., Wegener, G., Niemann, H., Deusner, C., Ferdelman, T.G., Boetius, A., Brunner, B., Widdel, F. (2011) Carbon and sulfur back flux during anaerobic microbial oxidation of methane and coupled sulfate reduction. *Proceedings of the National Academy of Sciences* 108, E1484-E1490.

Krüger, M., Meyerdierks, A., Glöckner, F.O., Amann, R., Widdel, F., Kube, M., Reinhardt, R., Kahnt, J., Böcher, R., Thauer, R.K. (2003) A conspicuous nickel protein in microbial mats that oxidize methane anaerobically. *Nature* 426, 878-881.

Lloyd, K.G., Alperin, M.J., Teske, A. (2011) Environmental evidence for net methane production and oxidation in putative ANaerobic MEthanotrophic (ANME) archaea. *Environmental Microbiology* 13, 2548-2564.

Marlow, J.J., Steele, J.A., Ziebis, W., Sheller, S., Case, D., Reynard, L.M., Orphan, V.J. (2017) Monodeuterated Methane, an Isotopic Tool To Assess Biological Metabolism Rates. *mSphere* 2, e00309-17.

Milucka, J., Ferdelman, T.G., Polerecky, L., Franzke, D., Wegener, G., Schmid, M., Lieberwirth, I., Wagner, M., Widdel, F., Kuypers, M.M. (2012) Zero-valent sulphur is a key intermediate in marine methane oxidation. *Nature* 491, 541-546.

Moran, J.J., House, C.H., Freeman, K.H., Ferry, J.G. (2005) Trace methane oxidation studied in several Euryarchaeota under diverse conditions. *Archaea* 1, 303-309.

Moran, J.J., House, C.H., Thomas, B., Freeman, K.H. (2007) Products of trace methane oxidation during nonmethyltrophic growth by Methanosarcina. *Journal of Geophysical Research: Biogeosciences* 112.

Niemann, H., Lösekann, T., De Beer, D., Elvert, M., Nadalig, T., Knittel, K., Amann, R., Sauter, E.J., Schlüter, M., Klages, M. (2006) Novel microbial communities of the Haakon Mosby mud volcano and their role as a methane sink. *Nature* 443, 854-858.

Piasecki, A., Sessions, A., Peterson, B., Eiler, J. (2016) Prediction of equilibrium distributions of isotopologues for methane, ethane and propane using density functional theory. *Geochimica et Cosmochimica Acta* 190, 1-12.

Regnier, P., Dale, A.W., Arndt, S., LaRowe, D., Mogollón, J., Van Cappellen, P. (2011) Quantitative analysis of anaerobic oxidation of methane (AOM) in marine sediments: a modeling perspective. *Earth-Science Reviews* 106, 105-130.

Scheller, S., Goenrich, M., Boecher, R., Thauer, R.K., Jaun, B. (2010) The key nickel enzyme of methanogenesis catalyses the anaerobic oxidation of methane. *Nature* 465, 606.

Scheller, S., Yu, H., Chadwick, G.L., McGlynn, S.E., Orphan, V.J. (2016) Artificial electron acceptors decouple archaeal methane oxidation from sulfate reduction. *Science* 351, 703-707.

Shima, S., Krueger, M., Weinert, T., Demmer, U., Kahnt, J., Thauer, R.K., Ermler, U. (2012) Structure of a methyl-coenzyme M reductase from Black Sea mats that oxidize methane anaerobically. *Nature* 481, 98.

Soo, V.W., McAnulty, M.J., Tripathi, A., Zhu, F., Zhang, L., Hatzakis, E., Smith, P.B., Agrawal, S., Nazem-Bokaee, H., Gopalakrishnan, S. (2016) Reversing methanogenesis to capture methane for liquid biofuel precursors. *Microbial cell factories* 15, 11.

Stolper, D.A., Martini, A.M., Clog, M., Douglas, P.M., Shusta, S.S., Valentine, D.L., Sessions, A.L., Eiler, J.M. (2015) Distinguishing and understanding thermogenic and biogenic sources of methane using multiply substituted isotopologues. *Geochimica et Cosmochimica Acta* 161, 219-247.

Thauer, R.K. (2011) Anaerobic oxidation of methane with sulfate: on the reversibility of the reactions that are catalyzed by enzymes also involved in methanogenesis from CO_2. *Current Opinion in Microbiology* 14, 292-299.

Timmers, P.H., Welte, C.U., Koehorst, J.J., Plugge, C.M., Jetten, M.S., Stams, A.J. (2017) Reverse Methanogenesis and respiration in methanotrophic archaea. *Archaea* 2017.

Valentine, D.L., Chidthaisong, A., Rice, A., Reeburgh, W.S., Tyler, S.C. (2004) Carbon and hydrogen isotope fractionation by moderately thermophilic methanogens. *Geochimica et Cosmochimica Acta* 68, 1571-1590.

Wang, D.T., Gruen, D.S., Lollar, B.S., Hinrichs, K.-U., Stewart, L.C., Holden, J.F., Hristov, A.N., Pohlman, J.W., Morrill, P.L., Könneke, M. (2015) Nonequilibrium clumped isotope signals in microbial methane. *Science* 348, 428-431.

Wang, D.T., Welander, P.V., Ono, S. (2016) Fractionation of the methane isotopologues 13 CH 4, 12 CH 3 D, and 13 CH 3 D during aerobic oxidation of methane by Methylococcus capsulatus (Bath). *Geochimica et Cosmochimica Acta* 192, 186-202.

Whiticar, M.J. (1999) Carbon and hydrogen isotope systematics of bacterial formation and oxidation of methane. *Chemical Geology* 161, 291-314.

Yan, Z., Joshi, P., Gorski, C.A., Ferry, J.G. (2018) A biochemical framework for anaerobic oxidation of methane driven by Fe (III)-dependent respiration. *Nature Communications* 9.

Yoshinaga, M.Y., Holler, T., Goldhammer, T., Wegener, G., Pohlman, J.W., Brunner, B., Kuypers, M.M.M., Hinrichs, K.U., Elvert, M. (2014) Carbon isotope equilibration during sulphate-limited anaerobic oxidation of methane. *Nature Geoscience* 7, 190-194.

Young, E., Kohl, I., Lollar, B.S., Etiope, G., Rumble, D., Li, S., Haghnegahdar, M., Schauble, E., McCain, K., Foustoukos, D. (2017) The relative abundances of resolved $^{12}CH_2D_2$ and $^{13}CH_3D$ and mechanisms controlling isotopic bond ordering in abiotic and biotic methane gases. *Geochimica et Cosmochimica Acta* 203, 235-264.

Exchange catalysis during anaerobic methanotrophy revealed by $^{12}CH_2D_2$ and $^{13}CH_3D$ in methane

J.L. Ash, M. Egger, T. Treude, I. Kohl, B. Cragg, J.R. Parkes, C.P. Slomp, B. Sherwood Lollar, E.D. Young

Supplementary Information

The Supplementary Information includes:

- Materials and Methods
- Tables S-1 to S-3
- Figures S-1 to S-3
- Supplementary Information References

Materials and Methods

Samples

Thermogenic Methane. Gases previously measured from the Marcellus and Utica Shales in the Appalachian Basin of the eastern USA are used as representative thermogenic gases in this study (Young *et al.*, 2017). The Marcellus formation consists of black, carbonaceous shale of Middle Devonian age, and the Utica formation (ranging from hundreds of meters to 2 km below the Marcellus) is an organic-rich, black calcareous shale of Middle Ordovician age. These samples originate from a well operated by Shell Oil Company in western Pennsylvania. Modern temperatures in the Marcellus and Utica Shales are 60 °C and 90 °C respectively (Rowan and Geological Survey (U.S.), 2006).

Methanogenesis cultures. Previously published clumped isotope data for axenic methanogen cultures are used as a reference in this study (Young *et al.*, 2017). The cultures were grown in crimp-top serum bottles at the University of Southern California. *Methanosarcina barkeri* and *Methanosarcina acetivorans* were grown at 30 °C with methanol. *Methanothermococcus thermolithotrophicus* was grown at 60 °C with CO_2 and H_2.

Baltic Sea. Baltic Sea methane samples analysed here were collected in October 2013 as part of the Integrated Ocean Drilling Program Expedition 347 (Baltic Sea Paleoenvironment). Sediment cores were drilled in Bornholm Basin (Site M0065; 55°28.034'N, 15°28.680'E). Sediment-associated methane was collected by plunging a cut-off, sterile syringe into a freshly exposed core end. Sediment samples of 5 cubic centimetres were extruded into 10 mL syringes pre-poisoned with 5 mL 1M NaOH and crimp sealed under atmosphere. Samples were agitated to break up sediment and stored upside down at 4 °C until analysis. Methane concentration and other key geochemical parameters were analysed as described in detail in (Egger *et al.*, 2017). Methane $\delta^{13}C$ and δD, $\delta^{13}C_{DIC}$, $\delta^{13}C_{TOC}$ and δD_{H2O} are shown in Figure S-1.

Abiotic methane synthesis. Methane samples produced through silane decomposition and the Sabatier reaction are representative of abiotically synthesised methane in this study. Details of these experiments are outlined in Young *et al.* (2017).

Kidd Creek Mine. Kidd Creek Mine extends to 3 km depth in the subsurface and the deepest waters sampled have billion-year residence times. Samples reported on within originate from two locations with depths of 7850 and 9500 feet and were collected from 2013-2015 (Young *et al.*, 2017). Temperatures range from 23-26 °C at the 7850 site and 29-32 °C at the 9500 site. Abiotic synthesis has been suggested to be the mechanism producing methane at a depth of 6800 feet (Sherwood Lollar *et al.*, 2002).

Stable and Clumped Isotope Notation

Stable isotope data is reported in delta notation where delta refers to a difference in rare isotope ratio from a standard. The standards include Pee Dee Belemnite (PDB) for carbon and Standard Mean Ocean Water (SMOW) for hydrogen. For example,

$$\delta^{13}\mathrm{C}=\left(\frac{^{13}R_{\mathrm{sample}}}{^{13}R_{\mathrm{standard}}}-1\right)\cdot 1000\ , \qquad \text{(Eq. S-1)}$$

where R refers to the ratio $^{13}\mathrm{C}/^{12}\mathrm{C}$ and the difference is in per mil (‰). Similarly, for D/H,

$$\delta\mathrm{D}=\left(\frac{^{2}R_{\mathrm{sample}}}{^{2}R_{\mathrm{standard}}}-1\right)\cdot 1000\ . \qquad \text{(Eq. S-2)}$$

Abundances of rare isotopologues are reported relative to the stochastic distribution of isotopic bond pairings in which the relative abundances of rare isotopologues are those predicted by chance for a given bulk isotopic composition. For example, the fraction of carbon that is the rare isotope, $^{13}\mathrm{C}$, is

$$X^{13}\mathrm{C}=\frac{^{13}\mathrm{C}}{^{13}\mathrm{C}+^{12}\mathrm{C}}\ , \qquad \text{(Eq. S-3)}$$

and the fraction of the hydrogen isotopes that is deuterium, D, is

$$X(\mathrm{D})=\frac{\mathrm{D}}{\mathrm{D}+\mathrm{H}}\ . \qquad \text{(Eq. S-4)}$$

In order to arrive at the stochastic distribution of isotopologues, the fractional abundances are equated with probabilities, yielding

$$X(^{12}\mathrm{CH}_4)=X(^{12}\mathrm{C})(X(\mathrm{H}))^4\ , \qquad \text{(Eq. S-5)}$$

$$X(^{13}\mathrm{CH}_4)=X(^{13}\mathrm{C})(X(\mathrm{H}))^4 \qquad \text{(Eq. S-6)}$$

and

$$X(^{12}\mathrm{CH}_3\mathrm{D})=4X(^{12}\mathrm{C})(X(\mathrm{H}))^4(X(\mathrm{D}))\ , \qquad \text{(Eq. S-7)}$$

where the coefficient "4" in Equation S-7 accounts for the four equivalent isotopomers created by varying configurations of D within molecules. This stochastic distribution of isotopes applies for systems in thermodynamic equilibrium at high temperatures

(>1000 K). At lower temperatures, thermodynamic equilibrium predicts excesses of the multiply-substituted species relative to stochastic.

As an example, consider the following intra-species isotope-exchange reaction:

$$^{13}CH_4 + {}^{12}CH_3D \rightleftharpoons {}^{13}CH_3D + {}^{12}CH_4 . \quad \text{(Eq. S-8)}$$

The equilibrium constant for this reaction is

$$K_{Eq} = \frac{\left[{}^{13}CH_3D\right]\left[{}^{12}CH_4\right]}{\left[{}^{13}CH_4\right]\left[{}^{12}CH_3D\right]} \quad \text{(Eq. S-9)}$$

where the brackets indicate molecular concentrations. The equilibrium constant at infinite temperature is evaluated by substituting the fractional abundances from Equation S-7 into Equation S-9 for the concentrations such that

$$K_{Eq} = \frac{4X(^{13}C)(X)(H))^3 X(D) X(^{12}C)(X(H))^4}{4X(^{12}C)(X)(H))^3 X(D) X(^{13}C)(X(H))^4} = 1 . \quad \text{(Eq. S-10)}$$

At temperatures lower than infinity, the equilibrium constant in Equation S-10 is >1. Values less than unity are indicative of kinetics, mixing, or some other process that shifts the abundances of isotopologues from their equilibrium values.

Per mil differences between the apparent intra-species equilibrium constant (concentration quotient) and the stochastic equilibrium constant are expressed using the capital delta notation such that

$$\Delta^{13}CH_3D = 10^3 \ln\left(\frac{K_{Eq}}{K_{Eq,Stochastic}}\right) \sim 10^3\left(\frac{X_{^{13}CH_3D}}{X_{^{13}CH_3D,Stochastic}} - 1\right) \approx 10^3\left(\frac{^{13}CH_3D R}{^{13}CH_3D R_{Stochastic}} - 1\right) . \quad \text{(Eq. S-11)}$$

The equivalent expression for $^{12}CH_2D_2$ is

$$\Delta^{12}CH_2D_2 = 10^3 \ln\left(\frac{K_{Eq}}{K_{Eq,Stochastic}}\right) \sim 10^3\left(\frac{X_{^{12}CH_2D_2}}{X_{^{12}CH_2D_2,Stochastic}} - 1\right) \approx 10^3\left(\frac{^{12}CH_2D_2 R}{^{12}CH_2D_2 R_{Stochastic}} - 1\right) . \quad \text{(Eq. S-12)}$$

Sample Purification and Analysis

Gas samples were purified on a vacuum line with inline gas chromatography using methods described previously (Young *et al.*, 2017). Mass spectrometric methods are similar to those previously described excepting the use of a small-volume cold finger during introduction to the bellows of the mass spectrometer inlet (Young *et al.*, 2016, 2017). In this modified method, samples are frozen onto a silica gel cold finger cooled by liquid nitrogen directly adjacent to the bellows housing for 5 minutes. The sample bellows and the cold finger are subsequently isolated from the rest of the dual inlet and warmed to room temperature. The variable volume bellows is cycled during warming to promote thorough mixing of gas. Between analyses, the cold finger is heated to 40 °C and pumped at high vacuum prior to introduction of new samples.

Baltic Sea samples for this study were analysed in July/August of 2016. A list of measured values for this study can be found in Table S-1. A tank methane gas (UCLA-2) was used as the reference internal standard. The composition of this gas was determined by comparing to gases of known bulk isotopic compositions and to gases heated to >800 °C. Aliquots of 30 to 60 µmol of UCLA-2 were repeatedly analysed during this session to assess external precision during measurement of Baltic Sea samples that were of comparable size. The average internal precisions (reported as 1σ) for $\delta^{13}C$, δD, $\Delta^{13}CH_3D$ and $\Delta^{12}CH_2D_2$ measurements are 0.004 ‰, 0.03 ‰, 0.32 ‰ and 0.85 ‰, respectively. External 1SD precisions for $\delta^{13}C$, δD, $\Delta^{13}CH_3D$ and $\Delta^{12}CH_2D_2$ values are 0.02 ‰, 0.05 ‰, 0.31 ‰ and 0.32 ‰ (n = 5).

To arrive at the total internal precision uncertainties listed above, the following error propagation was used. From Equation S-12, $\Delta^{12}CH_2D_2$ values are dependent on the measured $^{12}CH_2D_2/CH_4$ ratios and on the D/H ratios from the measured CH_3D/CH_4 ratios because

$$^{12}CH_2D_2R_{\text{Stochastic}} = 6\left(^{D}R\right)^2. \quad \text{(Eq. S-13)}$$

Therefore, the total uncertainty in $\Delta^{12}CH_2D_2$ is

$$\sigma^2_{\Delta^{12}CH_2D_2} = \left(\frac{\partial\Delta^{12}CH_2D_2}{\partial^{12}CH_2D_2R}\right)^2\sigma^2_{^{12}CH_2D_2R} + \left(\frac{\partial\Delta^{12}CH_2D_2}{\partial^{12}CH_2D_2R_{\text{Stochastic}}}\right)^2\sigma^2_{^{12}CH_2D_2R_{\text{Stochastic}}} \quad \text{(Eq. S-14)}$$

where the partial derivatives are

$$\frac{\partial\Delta^{12}CH_2D_2}{\partial^{12}CH_2D_2R} = \frac{10^3}{^{12}CH_2D_2R_{\text{Stochastic}}} \quad \text{(Eq. S-15)}$$

and

$$\frac{\partial\Delta^{12}CH_2D_2}{\partial^{12}CH_2D_2R_{\text{Stochastic}}} = -\frac{10^3\,^{12}CH_2D_2R}{\left(^{12}CH_2D_2R_{\text{Stochastic}}\right)^2}. \quad \text{(Eq. S-16)}$$

Standard errors in isotopologue ratios are derived from standard errors in the associated δ-values so that for the measured $^{12}CH_2D_2/CH_4$ ratio,

$$\sigma^2_{^{12}CH_2D_2R} = \left(\frac{\partial\,^{12}CH_2D_2R}{\partial\delta^{12}CH_2D_2}\right)^2\sigma^2_{\delta^{12}CH_2D_2} = \left(\frac{^{12}CH_2D_2R_{\text{Reference gas}}}{10^3}\right)^2\sigma^2_{\delta^{12}CH_2D_2} \quad \text{(Eq. S-17)}$$

where the partial derivative comes from the definition of the δ values. Likewise,

$$\sigma^2_{^{12}CH_2D_2R_{\text{Stochastic}}} = \left(\frac{\partial\,^{12}CH_2D_2R_{\text{Stochastic}}}{\partial^{D}R}\right)^2\sigma^2_{^{D}R} = \left(12\,^{D}R\right)^2\left(\frac{^{D}R_{\text{Reference gas}}}{10^3}\right)^2\sigma^2_{\delta D} \quad \text{(Eq. S-18)}$$

where Equations S-13 and S-2 are used to evaluate the partial derivative in Equation S-18. Finally, Equations S-15 through S-18 are substituted into Equation S-14. An analogous procedure applies to determine internal precision for $\Delta^{13}CH_3D$.

Methanogenesis rate measurements

At Cardiff University, samples for prokaryotic activity measurements were taken from the centre of whole-round cores with sterile 5 ml syringes (luer end removed) under anaerobic and aseptic handling conditions (Parkes *et al.*, 1995) and sealed with Suba-Seals (Sigma). All syringe mini-core samples were then equilibrated under anoxic conditions (under nitrogen in sealed gas-tight

aluminium bags) at 10 °C for approximately 12 h prior to further processing. Microbial activity was measured by injecting the syringe mini-core samples, along the central line of the syringe, individually with ^{14}C-acetate (7.5 µl, 81.3 kBq), ^{14}C-bicarbonate (7.5 µl, 106.2 kBq) or ^{14}C-dimethylamine (7.5 µl, 30.5 kBq) for estimating acetoclastic-, hydrogenotrophic-, and methylotrophic methanogenesis, respectively. All injected isotopes were in aqueous solution. Injected samples were then incubated at 10°C under anoxic conditions for a further 3, 7 and 16 h (^{14}C-acetate, -dimethylamine,) or 7, 16 and 24 h (^{14}C-bicarbonate). Ten syringe mini-cores were used at each depth for each isotope with one frozen immediately after injection as a control. Incubations were terminated by individually transferring the syringe contents into 30 ml glass vials containing 7 ml of 2 M NaOH, sealed, mixed thoroughly and stored inverted until processing. Radio-labelled methane was determined by purging the headspace (35 ml min^{-1} for 20 minutes) with a mixture of nitrogen and oxygen (95:5) as a carrier gas over copper oxide in a furnace (Carbolite, UK) at 900 °C and then into a CO_2 absorber.

Potential rates of methanogenesis for each substrate were determined by applying the label turnover rates to the pool size of total acetate, (DIONEX 2 x 50 mm guard column AG15 and 2 x 250 mm analytical column AS15 using KOH as eluent at a flow rate of 0.35 ml/min for 53 minutes with a conductivity detector and AERS-2 mm suppressor), dimethylamine (DIONEX 3 x 50 mm guard column CG16 and 3 x 250 mm analytical column CS16 using methanesulfonic acid as eluent at a flow rate of 0.36 ml/min for 80 minutes with a conductivity detector and CERS-2 mm suppressor), and CO_2 [calculated from IODP Expedition 347 pH and alkalinity data; (Andrén *et al.*, 2015)].

Sources of error for these measurements are principally that activity measurements were made *in vitro* after a period of sample storage, during which time super-saturated concentrations of methane in the core samples would have dissipated. Additionally, incubations were carried out at 10 °C under 1 atm pressure rather than *in situ* conditions. Measurements such as these are referred to as potential activity rates, and values are listed in Table S-2.

Modelling the timescale of equilibration

In order to assess the plausibility of equilibrating methane by methanotrophy in the Baltic Sea sediments, we determine the timescale necessary to equilibrate a hypothetical reservoir of methane with an initial clumped isotope composition identical to that produced by an axenic culture of *Methanosarcina acetivorans* grown on methanol at 30 °C ($\Delta^{13}CH_3D$ = -3.88‰ and $\Delta^{12}CH_2D_2$ = -40.86 ‰) (Young *et al.*, 2017). We determine the rate of enzymatic back reaction during AOM from the expression

$$R_{\text{-AOM}} = R_{\text{net AOM}} \left(\frac{R_-}{R_+} \right) \qquad \text{(Eq. S-19)}$$

where $R_{\text{-AOM}}$ is the enzymatic back reaction rate due to SO_4-AOM, $R_{\text{net AOM}}$ is the rate of net methanotrophy and $(R_-/R_+)_{AOM}$ is the ratio of enzymatic back reaction to net methanotrophy. For the value of $R_{\text{net AOM}}$, we take the weighted average flux of the present-day modelled rates from 10.33 MCD to 24.24 MCD, yielding 0.84 pmols CH_4 cm^{-3} d^{-1} (Dijkstra *et al.*). Values for $(R_-/R_+)_{AOM}$ from the literature range from 0.032 to 0.78 with an average value of 0.26 (Orcutt *et al.*, 2005; Seifert *et al.*, 2006; Treude *et al.*, 2007; Holler *et al.*, 2011; Yoshinaga *et al.*, 2014). These inputs suggest that a reasonable estimate for $R_{\text{-AOM}}$ for Bornholm Basin is 0.22 pmols cm^{-3} d^{-1}. The timescale (τ) of equilibration is determined from this rate estimate from the volumetric mixing ratio of methane:

$$\tau = \frac{[CH_4]}{R_{\text{-AOM}}} . \qquad \text{(Eq. S-20)}$$

From Equation S-20, the average timescale of equilibration for 5.36 mM CH4 (*i.e.* the methane concentration at 21.48 MCD) is ~ 6.7 x 10^4 years. For comparison, diagenetic porewater modelling suggests that the methane in equilibrium at a depth of 22 MCD should < ~8000 years. The difference between our estimate for equilibration time and the estimated age of the methane can be reconciled if:

1. $(R_-/R_+)_{AOM}$ for Fe-AOM in the Bornholm Basin is closer to (or greater than) the maximum measured value of 0.78 than the average value of 0.26 measured for SO_4-AOM,

or

2. The model $R_{net\ AOM}$ rates are underestimated.

Disentangling the contributions of the two potential sources of error to the calculated timescale is not possible *a priori*. However, modelled rates (*i.e.* net rates) are known to underestimate the actual turnover rates based on isotopic incubation studies (*i.e.* gross rates). Tripling $R_{net\ AOM}$ and using the higher value of 0.78 for $(R_-/R_+)_{AOM}$ decreases the calculated timescale of equilibration to 7.4 x 10^3 years, near to the estimated maximum age of the methane gas. Furthermore, these rates are unlikely to have been constant through time, and the present-day rates potentially overestimate rates of Fe-AOM and underestimate rates of SO_4-AOM through time (Dijkstra *et al.*, 2018).

In keeping with the implied uncertainties, we utilise a τ value of 10^4 years in the rate model used here for illustration purposes. The rate constant for enzymatic back reaction ($K_{\text{-AOM}}$) is obtained by treating the timescale of equilibration as an e-fold time:

$$K_{\text{-AOM}} = \frac{e}{\tau} \ . \qquad \text{(Eq. S-21)}$$

We utilise this $K_{\text{-AOM}}$ in a simple model that describes the equilibration from a disequilibrium methanogenic end member to thermodynamic equilibrium at the average temperature of 7.75 °C estimated from shipboard core temperature measurements. We describe the rate of equilibration system using

$$\frac{d\Delta}{dt} = K_{-AOM}(\Delta_{\text{Eq}} - \Delta_{\text{t}}) \ , \qquad \text{(Eq. S-22)}$$

where Δ_{Eq} is the clumped isotope composition at equilibrium and Δ_t is the clumped isotope composition at a given time step. In essence, this formulation treats the rate of reaction as one driven by the reaction affinity (*e.g.*, De Donder, 1927; Prigogine *et al.*, 1954).

The methanogenesis endmember defines $\Delta_{t=0,}$ and $\Delta_{t=\infty}$ is defined by thermodynamic equilibrium at 7.75 °C. The curves in Figure S-2 illustrate the timescales of equilibration for the two mass-18 isotopologues of methane. Figure S-3 shows the evolution of microbial methane progressively equilibrated over this timescale to the low-temperature AOM endmember in double isotopologue space under two treatments. The first assumes that $K_{\text{-AOM}}$ is equal for both the $^{13}CH_3D$ and $^{12}CH_2D_2$ isotopologues, and the trajectory is a straight line between the two endmembers. The second assumes that $K_{\text{-AOM}}$ for $^{12}CH_2D_2$ is half of that for $^{13}CH_3D$ to account for the higher energy barrier of bonding two deuteriums within a methane molecule.

Calculating $\xi_{^{12}CH_2D_2}$

The parameter $\xi_{^{12}CH_2D_2}$ quantifies the difference between $\Delta^{12}CH_2D_{2\_measured}$ and $\Delta^{12}CH_2D_{2\_equilibrium}$. $\Delta^{12}CH_2D_{2\_equilibrium}$ is calculated by assuming that for each datum, $\Delta^{13}CH_3D_{\_measured}$ is in equilibrium and that all methane isotopologues are in intra-species thermodynamic equilibrium. A $\xi_{^{12}CH_2D_2}$ value of zero implies that $\Delta^{12}CH_2D_{2\_measured}$ is in intra-species thermodynamic equilibrium with all methane isotopologues, and a positive or negative $\xi_{^{12}CH_2D_2}$ value implies that $\Delta^{12}CH_2D_{2\_measured}$ is not in intra-species thermodynamic equilibrium with the corresponding $\Delta^{13}CH_3D_{\_measured}$. In Bornholm Basin, the shallowest samples display the most negative values of $\xi_{^{12}CH_2D_2}$, and the deepest samples approach zero (Fig. 2).

Calculating ΔG of methane consumption

Here, both Fe-AOM and SO_4-AOM are potential methane consumption pathways. Evidence for enzymatic back-reaction during AOM with iron as the terminal electron acceptor has yet to be shown, but it has been suggested that the Gibbs free energies of reaction at standard conditions ($\Delta G°$=-16.3 kJ mol^{-1} for SO_4-AOM and $\Delta G°$=-571.2 kJ mol^{-1} for Fe-AOM) imply that Fe-AOM would be less reversible than SO_4-AOM, and therefore a weaker mechanism for equilibrating methane (Timmers *et al.*, 2017). However,

standard-state free energies of reaction are not the relevant indicators of reversibility. We calculate the Gibbs free energies of reaction ($\Delta G = \Delta G° + RT\ln Q$ where Q is the activity quotient for the reaction) for in-situ concentrations in the equilibrated methane zone (20 MCD) in Bornholm Basin and obtain values of -33.8 kJ mol^{-1} for SO_4-AOM and -93.4 kJ mol^{-1} for Fe-AOM (Table S-2). Although these estimates for ΔG values are still far from equilibrium, they are sufficiently close to one another to suggest that the likelihood of reversibility in SO_4-AOM and Fe-AOM are similar. Furthermore, it has been previously suggested that actual free energy dissipation during such reactions is less negative than suggested by calculations based on in-situ concentrations due to coupling to energy conservation (Holler *et al.*, 2011). This implies that enzymatic back-reaction may be possible in both Fe-AOM and SO_4-AOM even at these calculated Gibbs free energies.

We note that non-zero Gibbs free energies calculated from environmental conditions are related to the amount of energy available for microbial purposes (LaRowe and Amend, 2016) and can drive rates of reactions through reaction affinity in irreversible thermodynamics. However, they do not include the catalysing effects of the enzymes in the reaction. For instance, if one considers only Gibbs free energy as an indicator of reversibility, then the degree of reversibility of methanogenesis appears to be to that for anaerobic methanotrophy, implying back reaction is equally likely during both processes. However, this is contradictory to experiments that suggest the forward reaction is far more strongly favoured during methanogenesis (Moran *et al.*, 2005; Moran *et al.*, 2007), and the substantial clumped isotope evidence of disequilibrated methane produced by methanogens supports this conclusion (Stolper *et al.*, 2015; Wang *et al.*, 2015; Douglas *et al.*, 2016; Young *et al.*, 2017; Gruen *et al.*, 2018). In light of this, we infer that back reaction during methanogenesis (*i.e.* methane consumption) does not seem to be an important process in the subsurface for equilibrating methane isotopologues, and exploration of the intracellular metabolites that drive bi-bi reaction mechanisms at enzymes (Wongnate and Ragsdale, 2015) warrants further study.

Supplementary Tables

Table S-1 Potential activity measurements.

Depth (MCD)	Acetoclastic methanogensis activity pmol cm^{-3} d^{-1}	Hydrogenotrophic methanogenesis activity pmol cm^{-3} d^{-1}	Methylotrophic methanogenesis activity pmol cm^{-3} d^{-1}	Total methanogenesis activity pmol cm^{-3} d^{-1}
3.93	1.31	0.33	1.33	2.67
13.73	0.00	0.00	1.12	1.12
29.58	0.00	0.01	0.06	0.07
35.88	1.99	0.00	0.38	2.38

Table S-2 Species concentrations for ΔG calculations.

Reaction	Species	Concentration	Source
$CH_4 + SO_4^{2-} \rightarrow HCO_3^- + HS^- + H_2O_{(l)}$	SO_4^{2-}	0.16 mM	Andrén *et al.* (2015)
	HS^-	0.001 mM*	Egger *et al.* (2017)
	HCO_3^-	4.7 mM§	Egger *et al.* (2017)
	CH_4	5.36 mM	Andrén *et al.* (2015)
$CH_4 + 8Fe(OH)_{3(s)} + 16H^+ \rightarrow CO_2 + 8Fe^{2+} + 22H_2O_{(l)}$	Fe^{2+}	277.2 µM	Andrén *et al.* (2015)
	CH_4	5.36 mM	Andrén *et al.* (2015)
	H^+	$10^{-7.41}$ M¥	Andrén *et al.* (2015)
	CO_2	0.293 mM§	Egger *et al.* (2017)

* Below detection
§ Calculated from DIC concentration
¥ Calculated from shipboard pH measurements

Table S-3 Methane geochemistry of Bornholm Basin, Baltic Sea.

Depth (MCD)	$\delta^{13}C$ ‰ ± 2SE	δD ‰ ± 2SE	$\Delta^{13}CH_3D$ ± 2SE	$\Delta^{112}CH_2D_2$ ± 2SE
3.32	-76.16 ± 0.006	-244.03 ± 0.05	4.76 ± 0.43	7.88 ± 1.61
4.82	-74.06 ± 0.012	-242.45 ± 0.05	5.10 ± 0.69	8.52 ± 2.2
6.85	-72.54 ± 0.01	-239.91 ± 0.05	4.99 ± 0.66	11.79 ± 1.9
8.15	-71.81 ± 0.01	-238.60 ± 0.07	5.35 ± 0.67	11.42 ± 2.67
10.55	-71.87 ± 0.01	-239.34 ± 0.04	5.74 ± 0.59	15.13 ± 1.47
11.95	-72.11 ± 0.012	-239.95 ± 0.06	5.05 ± 0.56	14.48 ± 2.09
13.88	-72.33 ± 0.01	-239.21 ± 0.06	5.36 ± 0.61	16.70 ± 2.43
15.28	-72.89 ± 0.01	-238.91 ± 0.07	5.90 ± 0.68	17.43 ± 2.59
17.28	-74.03 ± 0.008	-238.37 ± 0.05	5.04 ± 0.46	16.21 ± 1.73
18.78	-74.63 ± 0.012	-238.28 ± 0.06	5.86 ± 0.55	16.72 ± 1.85
20.50	-75.59 ± 0.01	-238.20 ± 0.08	6.17 ± 0.61	20.54 ± 2.46

Supplementary Figures

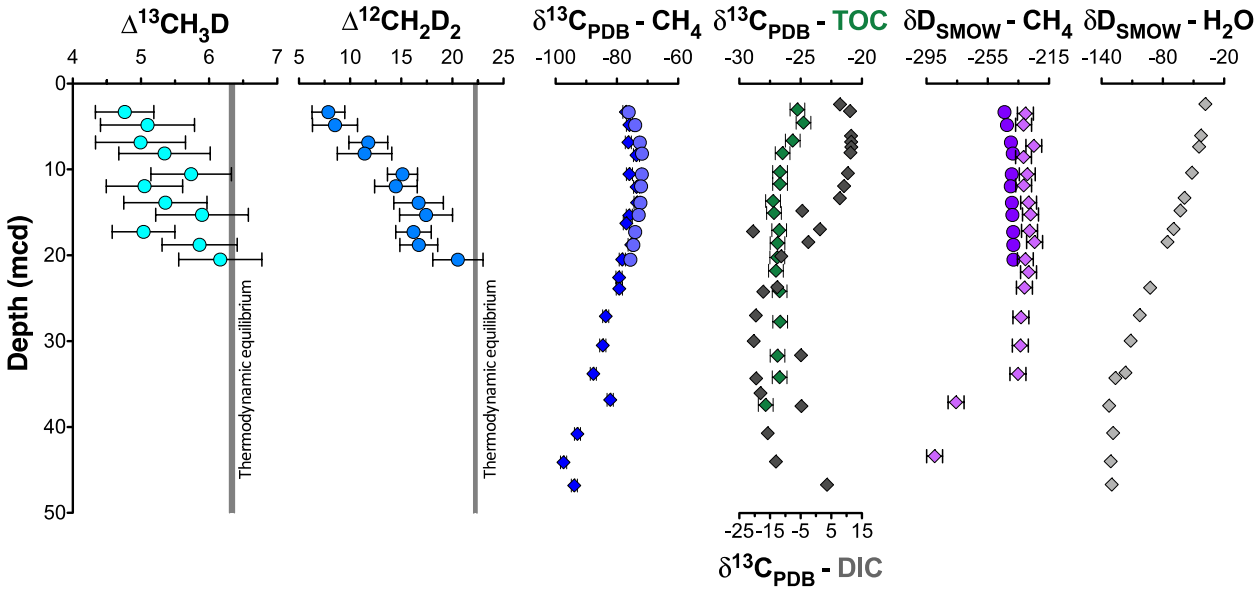

Figure S-1 Isotopes of methane, carbon and hydrogen reservoirs from Bornholm Basin, Baltic Sea are shown versus depth. Round symbols were measured in this study, diamond symbols are from previously published work (Egger *et al.*, 2017).

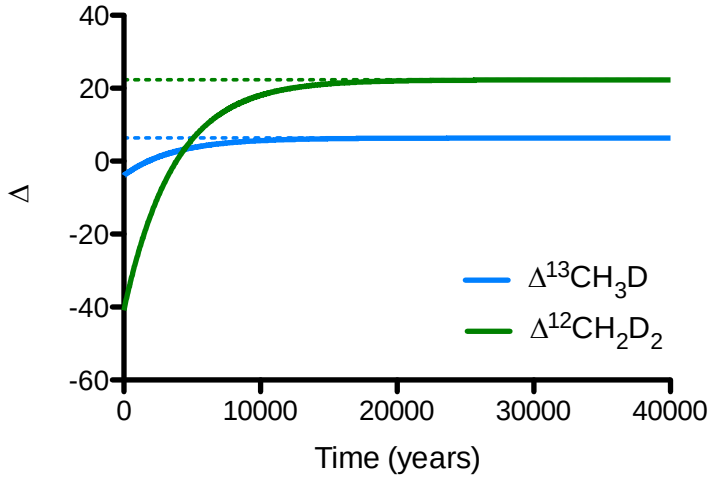

Figure S-2 $\Delta^{13}CH_3D$ and $\Delta^{12}CH_2D_2$ equilibrate within ~10,000 years. Equilibrium values for both species are shown as dashed lines.

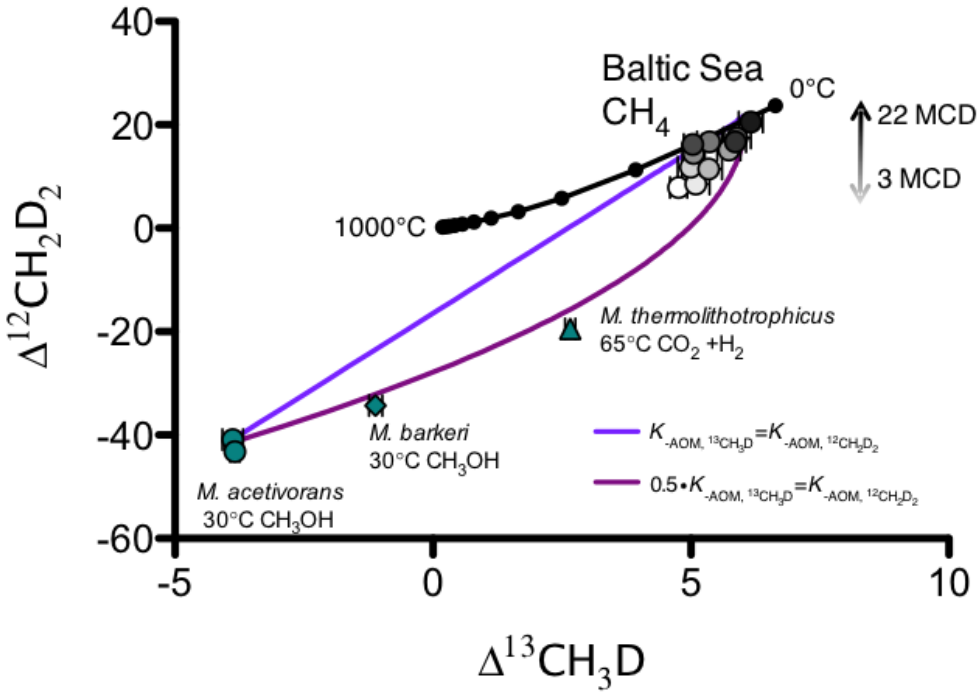

Figure S-3 $\Delta^{12}CH_2D_2$ is plotted versus $\Delta^{13}CH_3D$. Solid black line represents theoretical thermodynamic equilibrium in 100 °C increments marked by black circles. Baltic Sea methane data are shown as open circles shaded from white (shallowest sample) to black (deepest sample). Green symbols represent axenic cultures of methanogens as labeled. Purple lines represent equilibration pathways under two treatments as described in the text.

Supplementary Information References

Andrén, T., Jorgensen, B., Cotterill, C., Green, S., Andrén, E., Ash, J., Bauersachs, T., Cragg, B., Fanget, A., Fehr, A. (2015) Expedition 347 Baltic Sea Paleoenvironment. *Proceedings of the Integrated Ocean Drilling Program* 347, 1-66.

De Donder, T. (1927) *L'affinité*. Gauthier-Villars, Paris.

Dijkstra, N., Hagens, M., Egger, M., Slomp, C.P. (2018) Post-depositional vivianite formation alters sediment phosphorus records. *Biogeosciences* 15, 861-883.

Douglas, P., Stolper, D., Smith, D., Anthony, K.W., Paull, C., Dallimore, S., Wik, M., Crill, P.M., Winterdahl, M., Eiler, J. (2016) Diverse origins of Arctic and Subarctic methane point source emissions identified with multiply-substituted isotopologues. *Geochimica et Cosmochimica Acta* 188, 163-188.

Egger, M., Hagens, M., Sapart, C.J., Dijkstra, N., van Helmond, N.A., Mogollón, J.M., Risgaard-Petersen, N., van der Veen, C., Kasten, S., Riedinger, N. (2017) Iron oxide reduction in methane-rich deep Baltic Sea sediments. *Geochimica et Cosmochimica Acta* 207, 256-276.

Gruen, D.S., Wang, D.T., Könneke, M., Topçuoğlu, B.D., Stewart, L.C., Goldhammer, T., Holden, J.F., Hinrichs, K.-U., Ono, S. (2018) Experimental investigation on the controls of clumped isotopologue and hydrogen isotope ratios in microbial methane. *Geochimica et Cosmochimica Acta* 237, 339-356.

Holler, T., Wegener, G., Niemann, H., Deusner, C., Ferdelman, T.G., Boetius, A., Brunner, B., Widdel, F. (2011) Carbon and sulfur back flux during anaerobic microbial oxidation of methane and coupled sulfate reduction. *Proceedings of the National Academy of Sciences* 108, E1484-E1490.

LaRowe, D.E., Amend, J.P. (2016) The energetics of anabolism in natural settings. *The ISME journal* 10, 1285.

Moran, J.J., House, C.H., Freeman, K.H., Ferry, J.G. (2005) Trace methane oxidation studied in several Euryarchaeota under diverse conditions. *Archaea* 1, 303-309.

Moran, J.J., House, C.H., Thomas, B., Freeman, K.H. (2007) Products of trace methane oxidation during nonmethyltrophic growth by Methanosarcina. *Journal of Geophysical Research: Biogeosciences* 112.

Orcutt, B., Boetius, A., Elvert, M., Samarkin, V., Joye, S. (2005) Molecular biogeochemistry of sulfate reduction, methanogenesis and the anaerobic oxidation of methane at Gulf of Mexico cold seeps. *Geochimica et Cosmochimica Acta* 69, 5633-5633.

Parkes, R.J., Cragg, B.A., Bale, S., Goodman, K., Fry, J.C. (1995) A combined ecological and physiological approach to studying sulphate reduction within deep marine sediment layers. *Journal of Microbiological Methods* 23, 235-249.

Prigogine, I., Defay, R., Everett, D. (1954) *Chemical thermodynamics*. Longmans, Green London.

Rowan, E.L., Geological Survey (U.S.) (2006) Burial and thermal history of the central Appalachian Basin, based on three 2-D models of Ohio, Pennsylvania, and West Virginia*U S Geological Survey open-file report 2006-1019*. U.S. Dept. of the Interior, U.S. Geological Survey, Reston, Va.

Seifert, R., Nauhaus, K., Blumenberg, M., Krüger, M., Michaelis, W. (2006) Methane dynamics in a microbial community of the Black Sea traced by stable carbon isotopes in vitro. *Organic Geochemistry* 37, 1411-1419.

Sherwood Lollar, B., Westgate, T., Ward, J., Slater, G., Lacrampe-Couloume, G. (2002) Abiogenic formation of alkanes in the Earth's crust as a minor source for global hydrocarbon reservoirs. *Nature* 416, 522-524.

Stolper, D.A., Martini, A.M., Clog, M., Douglas, P.M., Shusta, S.S., Valentine, D.L., Sessions, A.L., Eiler, J.M. (2015) Distinguishing and understanding thermogenic and biogenic sources of methane using multiply substituted isotopologues. *Geochimica et Cosmochimica Acta* 161, 219-247.

Timmers, P.H., Welte, C.U., Koehorst, J.J., Plugge, C.M., Jetten, M.S., Stams, A.J. (2017) Reverse Methanogenesis and respiration in methanotrophic archaea. *Archaea* 2017.

Treude, T., Orphan, V., Knittel, K., Gieseke, A., House, C.H., Boetius, A. (2007) Consumption of methane and CO2 by methanotrophic microbial mats from gas seeps of the anoxic Black Sea. *Applied and Environmental Microbiology* 73, 2271-2283.

Wang, D.T., Gruen, D.S., Lollar, B.S., Hinrichs, K.-U., Stewart, L.C., Holden, J.F., Hristov, A.N., Pohlman, J.W., Morrill, P.L., Könneke, M. (2015) Nonequilibrium clumped isotope signals in microbial methane. *Science* 348, 428-431.

Wongnate, T., Ragsdale, S.W. (2015) The reaction mechanism of methyl-coenzyme M reductase: how an enzyme enforces strict binding order. *Journal of Biological Chemistry*, jbc. M115. 636761.

Yoshinaga, M.Y., Holler, T., Goldhammer, T., Wegener, G., Pohlman, J.W., Brunner, B., Kuypers, M.M.M., Hinrichs, K.U., Elvert, M. (2014) Carbon isotope equilibration during sulphate-limited anaerobic oxidation of methane. *Nature Geoscience* 7, 190-194.

Young, E., Kohl, I., Lollar, B.S., Etiope, G., Rumble, D., Li, S., Haghnegahdar, M., Schauble, E., McCain, K., Foustoukos, D. (2017) The relative abundances of resolved $^{12}CH_2D_2$ and $^{13}CH_3D$ and mechanisms controlling isotopic bond ordering in abiotic and biotic methane gases. *Geochimica et Cosmochimica Acta* 203, 235-264.

Young, E.D., Rumble, D., Freedman, P., Mills, M. (2016) A large-radius high-mass-resolution multiple-collector isotope ratio mass spectrometer for analysis of rare isotopologues of O_2, N_2, CH_4 and other gases. *International Journal of Mass Spectrometry* 401, 1-10.